Progress in Natural Science: Materials International 2013;23(6):598–607

Chinese Materials Research Society

Progress in Natural Science: Materials International

www.elsevier.com/locate/pnsmi
www.sciencedirect.com

ORIGINAL RESEARCH

Modeling the hot working behavior of near-α titanium alloy IMI 834

I. Balasundar[a,*], T. Raghu[a], B.P. Kashyap[b]

[a]*Near Net Shape Group, Aeronautical Materials Division, Defence Metallurgical Research Laboratory, Hyderabad 500058, India*
[b]*Department of Metallurgical Engineering and Materials Science, Indian Institute of Technology Bombay, Mumbai 400076, India*

Received 9 July 2013; accepted 1 September 2013
Available online 17 December 2013

KEYWORDS

Titanium alloys;
IMI 834;
Hot working;
Processing maps;
Constitutive modeling

Abstract The hot working behavior of near-α titanium alloy IMI 834 with a duplex starting microstructure was studied using the technique of processing map. The processing map was interpreted in terms of the microstructural processes occurring during deformation, based on the values of dimensionless parameter η which represents the energy dissipation through microstructural processes. An instability criterion ($\xi<0$) was also applied to demarcate the flow instability regions in the processing map. Both the parameters (η and ξ) were computed using the experimental data generated by carrying out hot compression tests over a range of temperatures (850–1060°C) and strain rates ($3 \times 10^{-4} - 1/\mathrm{s}$). The deterministic domains observed under the investigated temperature and strain rate conditions were attributed to continuous dynamic recrystallization or globularisation of α lamellae, dynamic recrystallization and growth of β grains through microstructural observations. An unified strain compensated constitutive equation was established to describe the hot working behavior of the material in the selected temperature–strain rate range. The established constitutive equation was validated using standard statistical parameters such as correlation coefficient and average absolute relative error.

1. Introduction

Titanium alloys are used extensively both as structural and engine component materials in aeroengines because of their high specific strength, high thermal stability and excellent corrosion resistance. Near-α titanium alloy IMI 834 is one such material that exhibits excellent creep and fatigue properties up to a temperature of 600°C [1–3]. Various rotor (discs, shafts and blades) and stator (rings and blades) components made out of this material are used in the high pressure compressor region of the aeroengines [4–7]. Vacuum arc melted and cast titanium alloys are generally subjected to thermomechanical processes such as hot forging [5], isothermal, near isothermal or hot die forging [6,8], ring rolling, roll forming [9] etc., to produce these critical class-I aeroengine components which require a combination of static and dynamic material properties [1–3]. It is important to understand the hot working behavior of the material in order to design

*Corresponding author. Tel.: +91 40 24586741; fax: +91 40 24340640.
E-mail address: i_balasundar@yahoo.com (I. Balasundar).

Peer review under responsibility of Chinese Materials Research Society.

ELSEVIER Production and hosting by Elsevier

1002-0071 © 2013 Chinese Materials Research Society. Production and hosting by Elsevier B.V. All rights reserved.
http://dx.doi.org/10.1016/j.pnsc.2013.11.004

a suitable process schedule to produce such critical aeroengine components. Appropriate selection of the thermomechanical processing parameters is also vital not only to attain the desired microstructure and mechanical properties but also to increase the efficiency and improve the quality of the product. Though the high temperature deformation behavior of the material has been reported earlier by various researchers [10–17], the thermomechanical processing parameters i.e., temperature, strain and strain rate required to produce various aeroengine components out of this material has not yet been identified or optimized. Even after identifying the optimum thermomechanical processing parameters, it is required to understand the deformation behavior of the material in the three dimensional deformation zone during metal forming where complicated state of stress (SOS) prevails. To address these issues and design a suitable deformation process, techniques such finite element analysis are generally used in the aerospace industry. The reliability of the output from finite element analyses depends to a large extent on the constitutive equations that are used to simulate the deformation behavior. Though various constitutive equations have been used to model the deformation behavior of hexagonal close packed materials [18–20], the phenomenological equation proposed by Sellars and Tegart [21,22] where the flow stress is expressed by a hyperbolic-sine function in an Arrhenius type equation has been found to predict and model the deformation behavior of a variety of materials quite reliably over many decades [23]. However, Sellars–Tegart [21,22] equation assumes that the strain rate has a greater influence on the flow stress when compared to strain. In case of titanium alloys, the microstructure evolution and hence the flow stress depends not only on temperature and strain rate but also on the strain [24,25] and strain path [26]. The dynamic recrystallization or globularisation behavior of transformed β structure has been found to be a function of strain in many Ti alloys [24–26]. Therefore, the effect of strain on the deformation behavior has to be incorporated into the constitutive equation [27,28] in order to model the deformation behavior accurately.

The objectives of the current study are: (1) to generate processing map to characterize the hot working behavior of near-α titanium alloy IMI 834 with a duplex microstructure using hot isothermal compression data, (2) to identify deformation mechanisms operating within various deterministic domains in the processing map by correlating the efficiency power of dissipation (η) to stress–strain response and as-deformed microstructure, (3) to establish the optimum thermomechanical processing parameters that can be used to design suitable process schedules to convert the material into useful aeroengine components and (4) to establish a suitable constitutive equation that considers the effect of temperature, strain rate and strain.

2. Dynamic materials modeling

Exhaustive information on the concept of dynamic materials modeling (DMM) can be found elsewhere [29]. According to this model, the workpiece is considered to be the dissipater of power. The total power P input to the material can be divided in to two complementary functions: G content and J co-content.

$$P = \sigma\dot{\varepsilon} = G + J = \int_0^{\dot{\varepsilon}} \sigma d\dot{\varepsilon} + \int_0^{\sigma} \dot{\varepsilon} d\sigma \tag{1}$$

where σ and $\dot{\varepsilon}$ represent the flow stress and strain rate respectively.

G content represents the power dissipated by plastic deformation most of which is converted in to heat whereas J co-content represents the power dissipated through microstructural changes. The power partitioning between G and J is controlled by the strain rate sensitivity (m). The metallurgical power dissipation processes may be characterized by the variation of J co-content with temperature and strain rate, but normalization with the input power sharpens the variation. This normalization leads to the definition of a dimensionless parameter called the efficiency (η) of power dissipation given as

$$\eta = \frac{J}{J_{\max}} = \frac{2m}{m+1} \tag{2}$$

The variation of η with temperature and strain rate constitutes the power dissipation map. Various domains in the map may be correlated with specific microstructural processes, which, in turn can be applied for controlling the same [29]. The stability condition described in the dynamic materials model by Kalyan Kumar [30] is based on the extremum principles of irreversible thermodynamics as applied to large plastic flow proposed by Ziegler [31]. The condition for microstructural stability at constant temperature, in terms of a dimensionless instability parameter ξ, is given by

$$\xi(\varepsilon) = \frac{\partial \ln(m/m+1)}{\partial \ln \dot{\varepsilon}} + m \tag{3}$$

Parameter ξ may be evaluated and plotted as a function of temperature and strain rate to obtain an instability map. Instabilities like adiabatic shear banding, flow localization, dynamic strain aging, mechanical twinning and kinking or flow rotations etc. have been reported to occur in regimes where ξ is negative [29]. Superimposition of the instability map over the power dissipation map gives the processing map.

3. Constitutive modeling

Sellars and Tegart hyperbolic-sine Arrhenius equation [21,22] has been widely employed to describe the relationship between the flow stress and processing parameters such as temperature and strain rate, at hot working conditions for various materials [23]. The effect of temperature and strain rate on the deformation behavior of the material is usually expressed using a temperature compensated strain rate parameter or Zener–Holloman parameter (Z) in an exponent-type equation:

$$Z = \dot{\varepsilon}\exp\left(\frac{Q}{RT}\right) \tag{4}$$

where $\dot{\varepsilon}$ is the strain rate (1/s), R is universal gas constant (8.314 J/mol K), T is the absolute temperature (K) and Q is the activation energy (J/mol) for hot deformation.

The strain rate and temperature dependence of stress is usually expressed as

$$\dot{\varepsilon} = A f(\sigma)\exp\left(\frac{-Q}{RT}\right) \tag{5}$$

$$f(\sigma) = \begin{cases} \sigma^{n'} & \text{for } \alpha\sigma < 0.8 \\ \exp(\beta'\sigma) & \text{for } \alpha\sigma > 1.2 \\ [\sinh(\alpha'\sigma)]^n & \text{for all } \alpha\sigma \end{cases} \tag{6}$$

where A, n', β', α' and n are material constants. n', β' and α' are related by $\beta' = \alpha' n'$ [21,22]. As the effect of strain is aimed to be incorporated into the constitutive equation, this can be achieved by expressing the constants as a function of strain [27,28].

4. Experimental procedure

Near-α titanium alloy IMI 834 with a nominal composition (wt%) of Ti - 5.8 Al - 4.0 Sn - 3.5 Zr - 0.7 Nb - 0.50 Mo - 0.35 Si - 0.06 C

in the as-forged and machined condition was procured from TIMET, UK, in the form of 172 mm diameter bars. The microstructure of the as-received material (Fig. 1) contains 35–40% primary alpha (Pα) in a transformed beta (Tβ) matrix. The variation in the size and shape of primary α present in the as-received material can be attributed to the local variation in the amount of deformation experienced by the material. The transformed β or the prior β grain size was found to vary from 40 to 65 μm. The average prior β grain size was estimated to be ≈ 50 μm. The as-received microstructure of the material used in the study is similar to that used by Bates et al. [10] except for the marginal variation in alloy chemistry and hence the variation in β transus temperature (β_t).

Isothermal hot compression tests were conducted over a range of temperatures and strain rates as shown in Table 1 to generate the high temperature flow data of the material. For compression testing, cylindrical samples with a constant height to diameter ratio of 1.5 were electro-discharge machined from the as-received bar and the edges of the machined samples were chamfered to avoid fold over during the initial stages of testing. A small hole of 0.8 mm in diameter, reaching to the center of the sample was drilled at its mid-height and a K-type thermocouple was inserted through it to monitor and record the temperature. Deltaglaze 347 coated IMI 834 samples were then heated to the deformation temperature at a rate of 5°C/min using a split type resistance heating furnace, held for 30 min and compressed under constant true strain rates on a computer controlled servo-hydraulic testing machine, custom built by DARTEC, UK. The adiabatic temperature rise during deformation was recorded. After testing, the samples were water quenched to freeze the high temperature microstructure. The quenched samples were then cut parallel to compression direction. The cut faces were then polished and etched with Kroll's reagent for microstructural evaluation using an optical microscope.

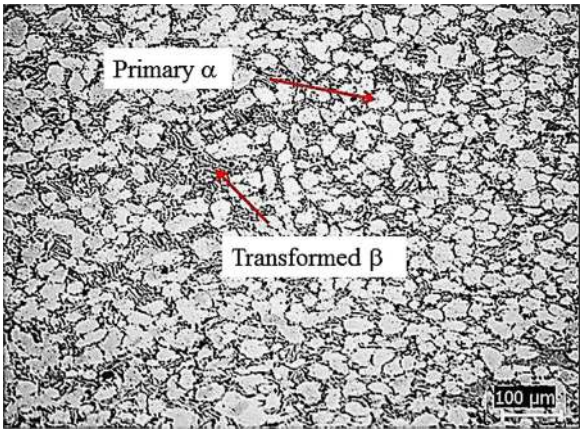

Fig. 1 Typical microstructure of the as-received IMI 834 material exhibiting duplex microstructure.

Table 1 Temperature and true strain rate domain considered for processing map generation.

Material: near-α titanium alloy IMI 834	
Temperature (°C)	850, 900, 950, 1000, 1030, 1060
Strain rate (1/s)	3×10^{-4}, 10^{-3}, 10^{-2}, 10^{-1}, 1
% Reduction in height	50% ≡ True strain (ε): 0.694

The load-stroke curves obtained after compression testing were converted to true stress–true strain curves using standard procedures reported elsewhere [29]. The elastic strain region was removed to obtain true stress–true plastic strain curves. The flow stress at each true plastic strain was then corrected for adiabatic temperature rise (ATR) by applying linear interpolation and extrapolation between flow stress and inverse of temperature on a semi-log scale as discussed elsewhere [29]. From the ATR corrected flow stress, the temperature sensitivity parameter [31] or entropy production rate (S) and the strain rate sensitivity of the material were evaluated using the equations listed below

$$S = \frac{1}{T}\left(\frac{\partial \log \sigma}{\partial(1/T)}\right) \tag{7}$$

$$m = \frac{\partial \ln \sigma}{\partial \ln \dot{\varepsilon}} \tag{8}$$

Standard cylindrical tensile samples of 6 mm diameter and 30 mm gage length were prepared from the as-received material and tested at predetermined temperature and strain rate (discussed later) using INSTRON 1185 universal testing machine as per American Standards for Testing and Materials (ASTM) E21 [32].

5. Results and discussions

5.1. *True stress–true strain curves*

Typical true stress–true strain curves generated by converting the load–stroke curves obtained from the hot compression tests are illustrated in Fig. 2a–f. Samples deformed at 850 and 900°C, exhibit flow softening following the peak in flow stress that occurs in the early stage of deformation. Eventually the flow stress generally reaches a steady state at strain ≥ 0.60, depending on the strain rate. At 950 and 1000°C, the material exhibits steady state behavior at lower strain rates ($3 \times 10^{-4} - 10^{-2}$/s) and flow softening characteristics at high strain rates ($10^{-1} - 1$/s). The peak stress was found to increase with strain rate and decrease with temperature. Yield drop and serrations were observed in true stress–true strain curves when deformed between 1030 and 1060°C. The occurrence of the yield drop and serrations can be attributed to the high solute content ($\approx 15\%$) and the large atomic size difference of carbon and silicon with respect to that of titanium as explained by Wanjara et al. [12]. The effect of deformation temperature on the initial microstructure of the material is shown in Fig. 3a–d. The variation of primary α with temperature (Fig. 3a–d) was estimated using point count technique [32]. From the primary α volume fraction, the volume fraction of β phase was estimated (β volume fraction = 100 − primary α volume fraction) and is shown in Fig. 3e in comparison with that reported in literature [2,3,11,17].

5.2. *Effect of temperature*

The effect of temperature on the flow stress of the material at a true strain of 0.5 is shown in Fig. 4a. For deformation temperatures ≥ 1030°C, the flow stress is less sensitive to temperature whereas below this temperature it is highly temperature sensitive. Though Weiss and Semiatin [33] have reported that such a transition in flow

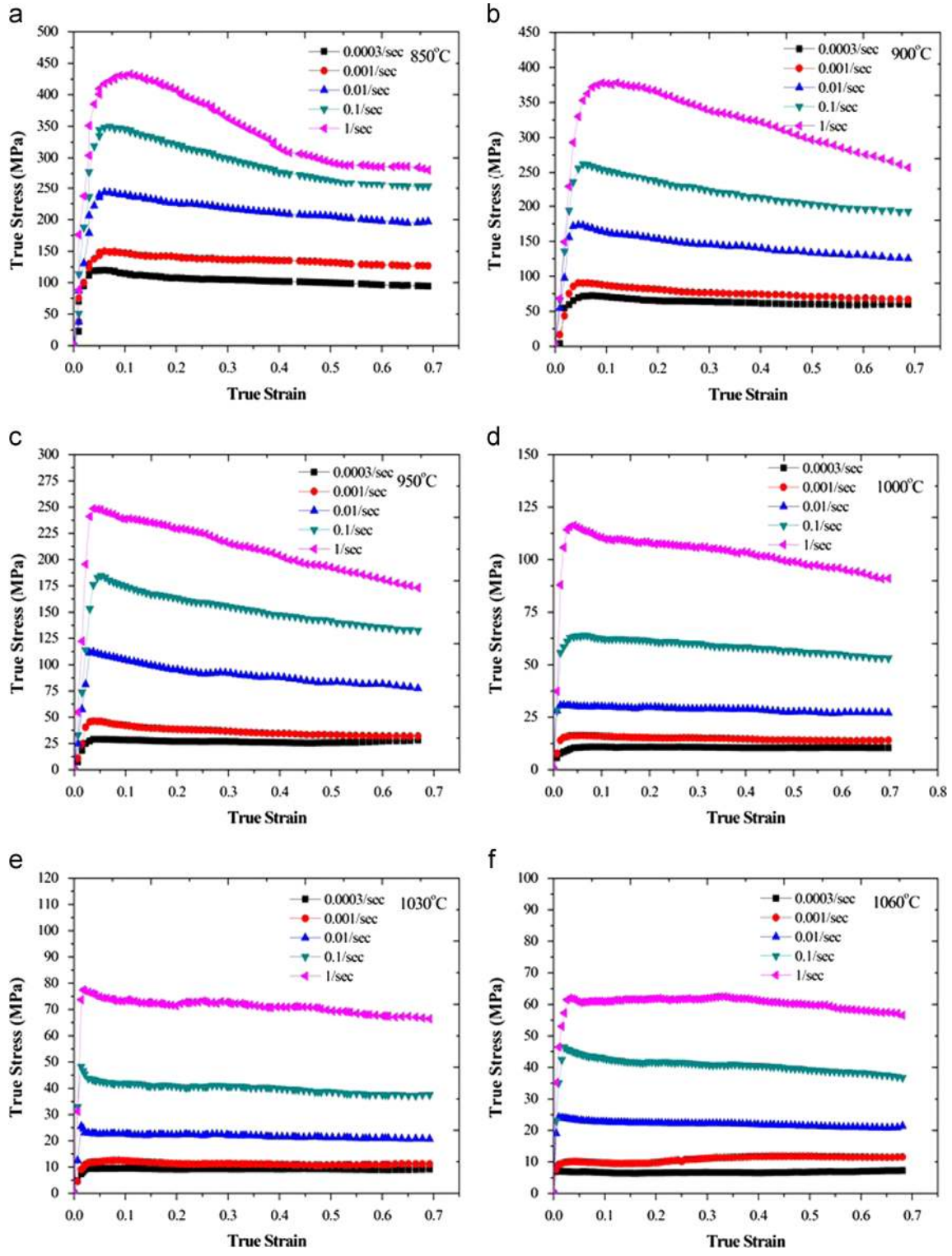

Fig. 2 True stress–true strain curves for IMI 834 with a duplex starting microstructure obtained by hot compression testing at various temperature and constant true strain rates.

stress temperature sensitivity takes place at the β transus of the material, it is observed at much lower temperature between 1000 and 1030°C (β_t–[70 to 40°C]) here concurring with the findings of Wanjara et al. [12]. At temperatures less than 1030°C, HCP α phase controls the deformation behavior whereas at temperature > 1030°C, the BCC β being the dominant phase controls the deformation. The qualitative (Fig. 3a–d) and quantitative (Fig. 3e) variation of the as-received microstructure with hot working temperature concurs well with above mentioned statement.

During deformation, the material dissipates the instantaneous power by metallurgical processes commensurate with the level of power applied. The applied power induces an entropy production

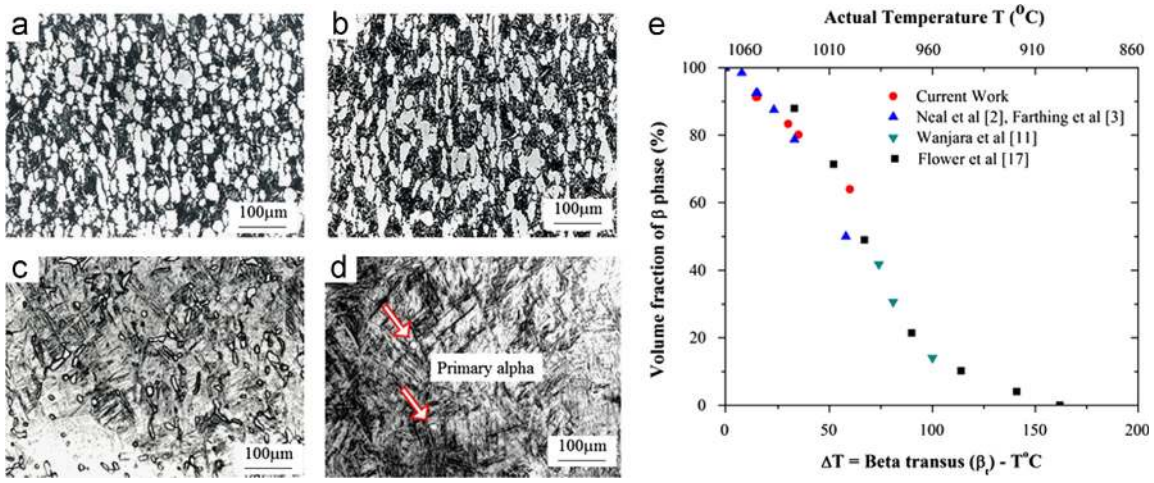

Fig. 3 Variation in the microstructure of as-received material with respect to hot working temperature (a) 850°C, (b) 950°C, (c) 1030°C, (d) 1060°C and (e) quantitative variation of β volume fraction with temperature.

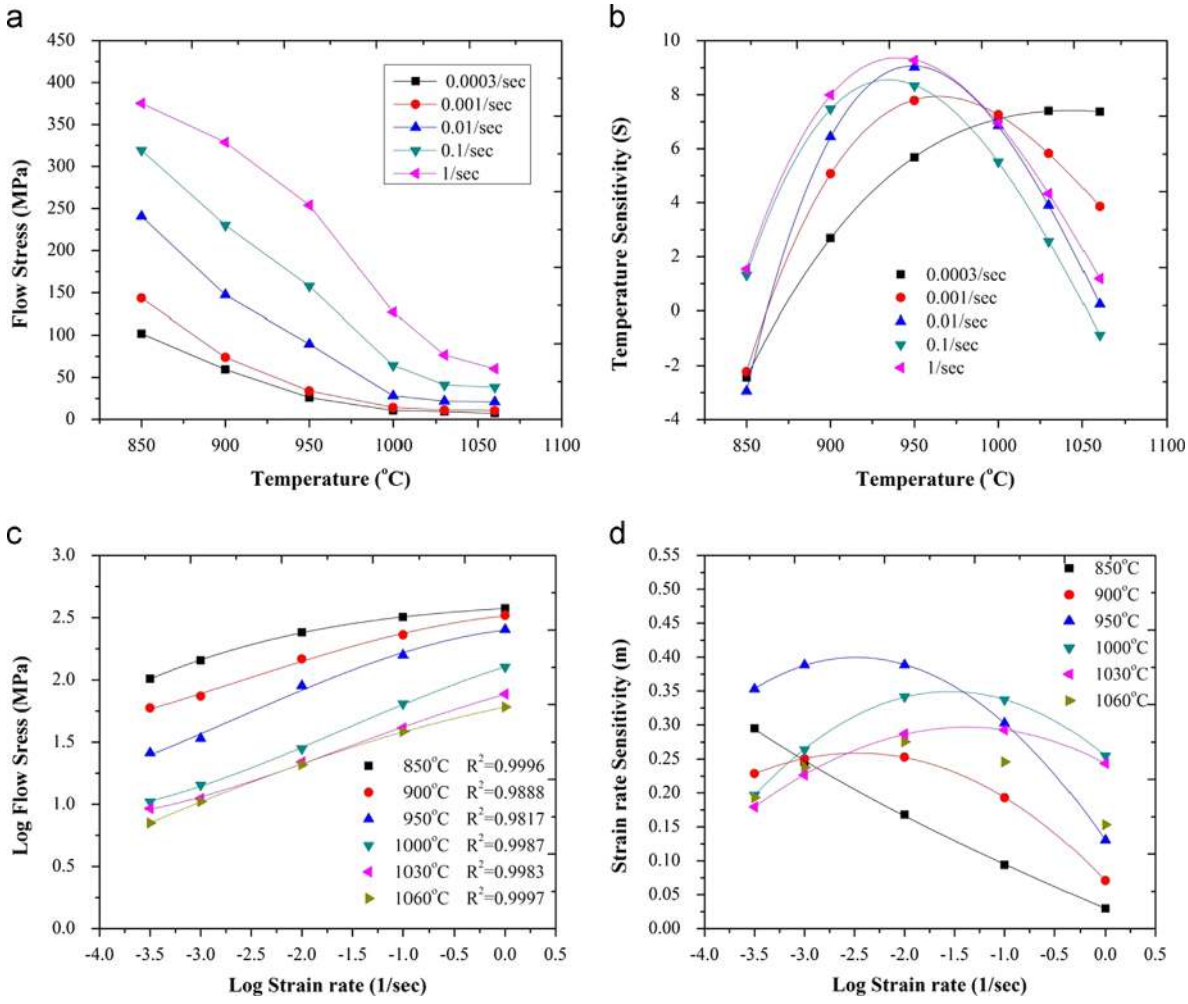

Fig. 4 (a) Variation of flow stress with temperature, (b) variation of temperature sensitivity parameter or the entropy production rate (*S*) with temperature, (c) variation in flow stress as a function of strain rate on log–log scale and (d) variation in strain rate sensitivity *m* with strain rate.

rate which is controlled by the second law of thermodynamics and is directly related to the grain size [34]. The rate of entropy production by the material reaches a maximum when the material has the potential to develop very fine grain size [34]. The rate of entropy production decreases when grain growth takes place. Entropy production rate ratio (*S*) calculated for the material at a true plastic strain of 0.5 using Eq. (7) is plotted against the deformation temperature in Fig. 4(b). It can be seen that,

irrespective of the strain rate, the entropy rate ratio reaches to a peak value at intermediate temperatures (900–1000°C). The material is expected to exhibit a fine grain structure in this temperature range since the parameter S is directly correlated to the additional area per unit volume created during deformation [34]. At lower temperature (850°C) and higher strain rates ($10^{-3}-1/s$), and higher temperature (1060°C) and lower strain rates ($3\times10^{-4}-10^{-3}/s$) the entropy rate ratio is less than 1. Under these processing conditions the material is expected to exhibit unstable flow in the form of instabilities or grain growth [34] these aspects are discussed later when correlating the domains in the processing map with the microstructural observations.

5.3. *Effect of strain rate*

The variation in flow stress as a function of strain rate, for a true plastic strain of 0.5 is plotted on a log–log scale as shown in Fig. 4(c). The strain rate sensitivity (m) that corresponds to the slopes of these curves is shown in Fig. 4(d). The material exhibits two strain rate sensitivity peaks, one at 950°C and at a strain rate of $3\times10^{-3}/s$ and the other at 1000°C and at the strain rate of $3\times10^{-2}/s$. The peak values of m under these conditions are found to be 0.40 and 0.33 respectively.

5.4. *Processing map*

The processing map developed for the material plotted for a true plastic strain of 0.6 is shown in Fig. 5. The shaded and un-shaded regions in the processing map represent unstable and stable flow regimes respectively.

5.4.1. *Instability region*

In the unstable region, the material exhibits instability in the form of shear bands. At certain combinations of temperature and strain rate, the temperature of the sample during deformation increased beyond the deformation temperature during compression testing. For example, when deformed at 850°C and 1/s, the temperature of the sample increased to 57°C. The temperature rise measured here is within the range estimated and reported by Li et al. [35] and Niu et al. [36] for near-α titanium alloys. The shear band instability (Fig. 6a) observed in the region can be attributed to this adiabatic temperature rise. At high strain rates, adiabatic heat generated during deformation is not conducted away due to insufficient time and low thermal conductivity of titanium alloys. As the temperature is increased by adiabatic heating, the flow stress required for deformation decreases and hence localization of deformation takes place leading to the formation of such bands [29,33]. IMI 834 should not be processed under these temperature–strain rate regime to avoid inhomogeneous deformation of the material.

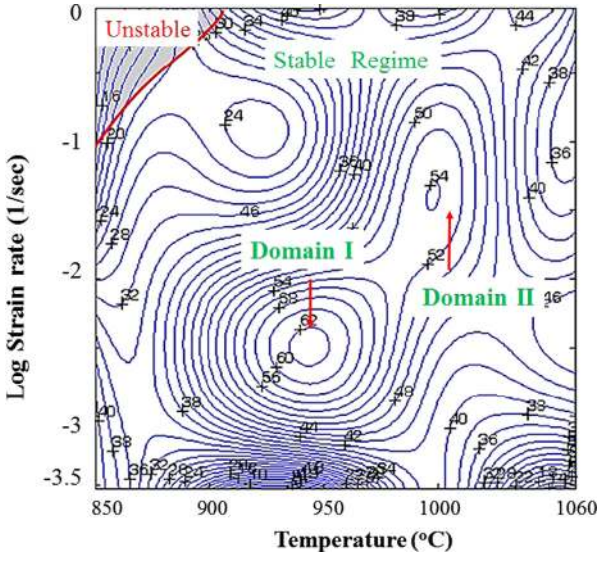

Fig. 5 Processing map for IMI 834 material with a duplex microstructure (35–40% Pα in a Tβ matrix) at a true plastic strain of 0.6 showing two deterministic domains.

5.4.2. *Stable flow regime*

In the stable region, the map exhibits two domains. As per dynamic materials modeling (DMM), domains are the regions where deterministic deformation mechanisms operate [29]. The first deterministic domain is observed in the temperature range of 925–975°C and strain rate range of $10^{-3}-10^{-2}/s$ with a maximum efficiency of 62%. The efficiency values in the domain increase steeply. The material exhibits high strain rate sensitivity (Fig. 4d) and entropy rate ratio (Fig. 4b) in the domain. The deformed material exhibits a fine microstructure as compared to the as-received microstructure and to those microstructures obtained when processed outside the domain. The microstructure consists of coarse primary α particles in a transformed β matrix along with fine dynamically recrystallized or globularised α particles from the lamellar structure as shown in Fig. 6b. The mechanism of globularisation of lamellar α is similar to that proposed by Weiss et al. [37] and the same are discussed elsewhere [32]. The process of globular α particle formation from the lamellar α is referred as continuous dynamic recrystallization (CRDX) [29,38].

Based on the microstructure obtained, the sharp increase in the efficiency and the high strain rate sensitivity observed in the domain (925–975°C; $10^{-3}-10^{-2}/s$), the material can be expected to exhibit superplastic characteristics [8]. For instance, a total elongation of 110% was obtained by tensile testing at 950°C and an average strain rate of $3.16\times10^{-3}/s$ (Fig. 7a) with $m\approx0.40$ (Fig. 4d). To some extent this substantiates the fact that the material exhibits superplastic characteristics. However, the maximum ductility attained here is less than that reported for the superplastic grade material [39]. This can be attributed to the bimodal (coarse and fine primary α) microstructure present in the material and to the growth of the primary α phase during tensile testing. As the cross head speed during tensile testing is held constant, the true strain rate decreases during a tensile test. When the material is deformed at 950°C with a slow strain rate, coalescence and growth of the primary α phase takes place as shown in Fig. 6c. This growth in the α phase during tensile testing could restrict the maximum elongation that can be achieved.

The second domain in the processing map (Fig. 5) is observed between 980 and 1020°C and $10^{-2}-10^{-1}/s$ with a maximum efficiency of 54%. At 975°C and a strain rate of $10^{-2}/s$, the material exhibits high entropy rate ratio (Fig. 5b) which is correlated to the additional interface area created per unit volume during dynamic recrystallization. The strain rate sensitivity is found to be 0.35 in this temperature–strain rate regime. The microstructure of the deformed sample shows a partially dynamic recrystallized β structure with wavy grain boundaries (Fig. 8a). It can therefore be stated that the material undergoes dynamic

β recrystallization in this domain. A total elongation of 80% (Fig. 7a) exhibited by the material when tested under tension in this temperature–strain rate regime and a fine transformed β grain size (∼40–80 μm) obtained when the partially dynamic recrystallized sample is subjected to static recrystallization (SRX) supports the argument that the material undergoes dynamic recrystallization (β DRX) in this domain. Irrespective of the temperature–strain rate domain, the % elongation increases with increasing efficiency (Fig. 7b) of power dissipation.

In the processing map (Fig. 5), the power dissipation efficiency (η) value decreases as the deformation temperature beyond 1030°C at almost all strain rates. The strain rate sensitivity is less in

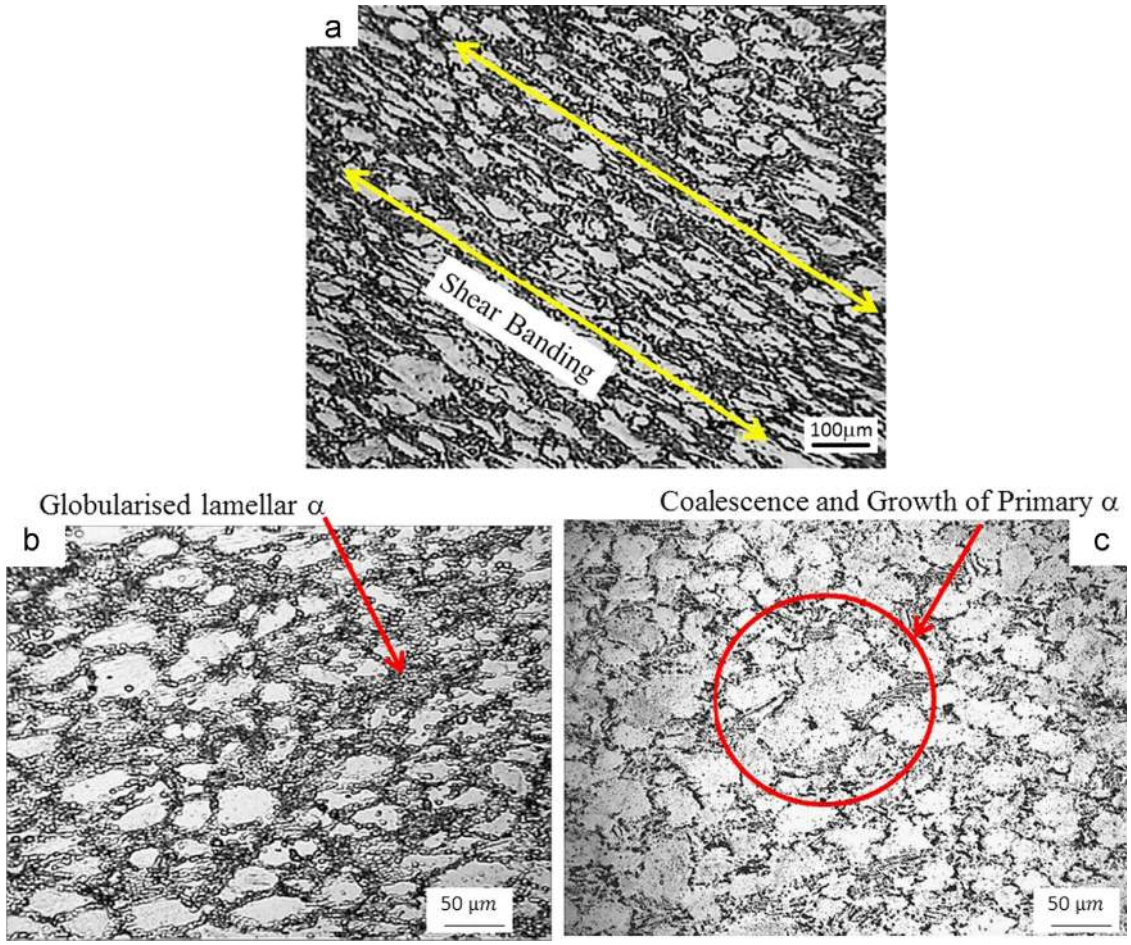

Fig. 6 Microstructure of the material deformed (a) at 850°C and 1/s showing adiabatic shear bands, (b) at 950°C and 10^{-2}/s showing completely globularised or CDRX of α lamellae (c) at 950°C and 3×10^{-4}/s exhibiting coalescence and growth of primary α.

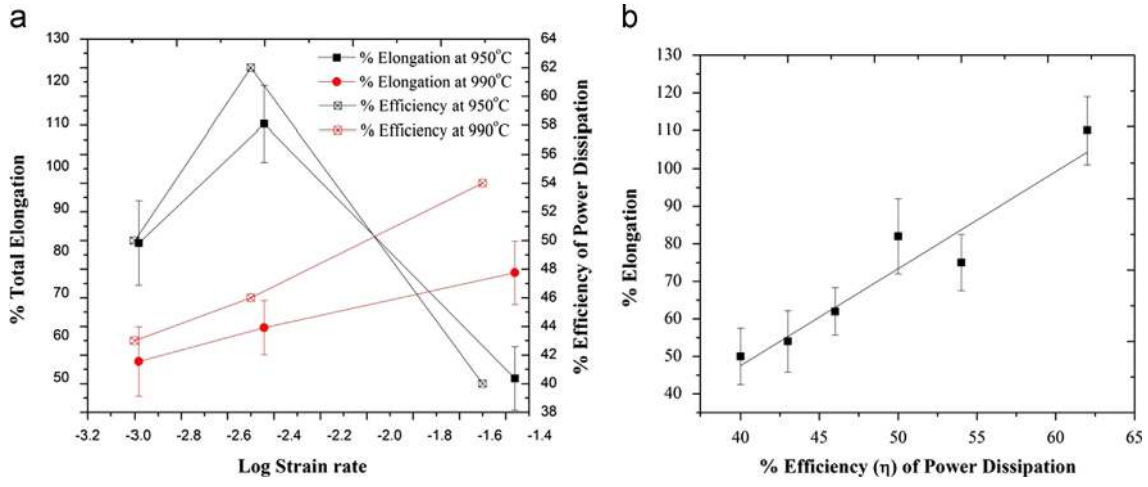

Fig. 7 Variation of (a) power dissipation efficiency (η) and total elongation with strain rate (b) % elongation with efficiency of power dissipation.

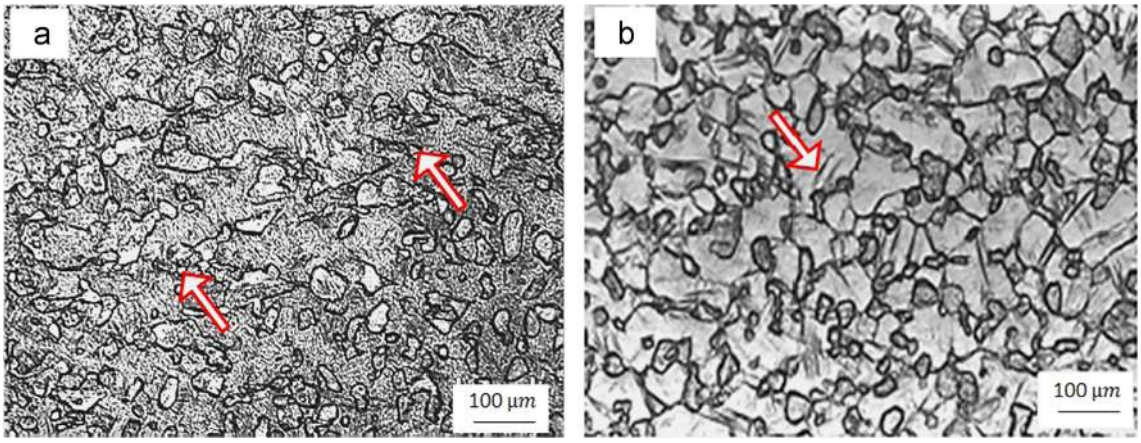

Fig. 8 Microstructure of the material deformed at (a) 1000°C and 10^{-1}/s showing partial DRX of beta grains (b) 1030°C and 3×10^{-4}/s showing completely RX and grown beta grains. (In the above figure, the partial DRX, completely RX and grown β grains are identified using arrows).

Table 2 Manifestations in IMI 834 during hot working at various temperature–strain rate regime.

Manifestation	Temperature (°C)	Strain rate (1/s)
Shear banding	850–925	$10^{-1} - 1$
Pseudo superplastic/lamellar α globularisation/continuous dynamic recrystallization (CDRX) regime	920–975	$10^{-3} - 10^{-2}$
Dynamic β recrystallization	980–1020	$10^{-2} - 10^{-1}$

this temperature range when compared to the peak values. The microstructure of the samples processed under these conditions exhibit larger prior β grains. The entropy production rate in this region also decreases with increasing temperature (Fig. 4d) and values less than 1 (unstable flow) were obtained for certain strain rates. The sample deformed in this region (1030°C and at 3×10^{-4}/s) exhibits larger transformed β grain size as shown in Fig. 8b. Therefore, final processing of the material above 1020°C at strain rates $\leq 10^{-3}$/s is not recommended. If processed, then stress assisted grain growth of dynamically recrystallized β phase would take place, which is then difficult to refine during the post deformation heat treatments. The micro-mechanisms observed in the material at various temperature and strain rate regions are summarized in Table 2. This information can be used to choose the optimum processing parameters and design a suitable process based on the equipment available, final microstructure and properties that are required.

5.5. *Constitutive modeling*

To establish a constitutive equation that can be used in various finite element codes to simulate the thermo-mechanical behavior of the material under a given state of stress, the materials constants in Eq. (6) are to be established as a function of strain. The procedure used to estimate the material constants at a true plastic strain of 0.5 is listed below. Substituting the value of $f(\sigma)$ at low and high stress levels in Eq. (5) gives

$$\dot{\varepsilon} = B\sigma^{n'} \tag{9}$$

$$\dot{\varepsilon} = C \exp(\beta'\sigma) \tag{10}$$

where B and C are material constants. Taking logarithm on both sides reduces Eqs. (9) and (10) to represent a straight line. The value of n' and β' are then obtained from the slope of $\ln(\sigma)$ vs. $\ln(\dot{\varepsilon})$, and σ vs. $\ln(\dot{\varepsilon})$ plots. As the straight lines are apparently parallel, the mean values of slopes are taken as $n'$and β'. The value of n' and β' are estimated to be 4.15 and 0.073 MPa^{-1} respectively at a true plastic strain of 0.5. The value of α' is then estimated from $\alpha' = (\beta'/n') = 0.0176$.

For low and high flow stress, the constitutive equation is given as

$$\dot{\varepsilon} = A[\sinh(\alpha\sigma)]^n \exp\left(-\frac{Q}{RT}\right) \tag{11}$$

Taking logarithm on both sides and rearranging gives

$$\ln[\sinh(\alpha\sigma)] = \frac{\ln\dot{\varepsilon}}{n} + \frac{Q}{nRT} - \frac{\ln A}{n} \tag{12}$$

Differentiating Eq. 12 w.r.t. $\ln(\dot{\varepsilon})$ and $1/T$ gives

$$\frac{1}{n} = \frac{d\{\ln[\sinh(\alpha\sigma)]\}}{d\{\ln\dot{\varepsilon}\}} \tag{13}$$

$$Q = Rn\frac{d\ln[\sinh(\alpha\sigma)]}{d\left(\frac{1}{T}\right)} \tag{14}$$

The value of the stress exponent (n) and activation energy (Q) are obtained from the slopes of $\ln[\sinh(\alpha\sigma)]$ vs. $\ln(\dot{\varepsilon})$ and $\ln[\sinh(\alpha\sigma)]$ vs. $1/T$ plots respectively. The stress exponent (n) and apparent activation energy (Q) estimated at a true plastic strain of 0.5 were found to be 2.25 and 672 kJ/mol. The activation energy estimated here is well within the range reported for dynamic recrystallization for such materials as shown in Table 3. The value of A (6.97×10^{25}/s) is estimated from the intercept value of Fig. 9b. The aforementioned procedure was repeated to estimate the material constants at lower true strains of 0.1, 0.2, 0.3 and 0.4. The corresponding values of material constants are listed in Table 4. A third order polynomial equation was found to satisfactorily express the variation of material constants within the strain range of 0.1 to 0.5 as shown Fig. 9a–d. The strain

compensated constitutive equation to estimate the flow stress is therefore given by

$$\sigma = \frac{1}{\alpha'} \ln\left\{ \left(\frac{Z}{A}\right)^{1/n} + \left[\left(\frac{Z}{A}\right)^{2/n} + 1\right]^{1/2} \right\} \quad (15)$$

where, Z, A, n and α' are expressed as function of strain as shown in Fig. 9a–d.

The reliability of the constitutive equation established here (Eq. (15)) in estimating the flow stress for a given processing condition can be verified and validated using standard statistical parameters such as correlation coefficient (R^2) and average absolute relative error (AARE) [27,28]. These are expressed as

$$R^2 = \frac{\sum_{i=1}^{N}(E_i - \overline{E})(P_i - \overline{P})}{\sqrt{\sum_{i=1}^{N}(E_i - \overline{E})^2 \sum_{i=1}^{N}(P_i - \overline{P})^2}} \quad (16)$$

$$\text{AARE}\,(\%) = \frac{1}{N}\sum_{i=1}^{N}\left|\frac{E_i - P_i}{E_i}\right| \times 100 \quad (17)$$

where E is the experimental flow stress and P is the predicted flow stress obtained from the strain compensated constitutive equation established here. $\overline{E}$ and $\overline{P}$ are the mean values of E and P respectively. N is the total number of data used in this study. Correlation coefficient R^2 provides information on the strength of the linear relationship between the experimental and predicted flow stress. It has been reported that a higher value of correlation coefficient (R^2) need not imply better performance [28] because of the tendency of R^2 to be biased towards higher or lower values. The average absolute relative error (AARE) is calculated through a

Table 3 Activation energy reported for IMI 834 and other near-α titanium alloys.

Material and reference	Beta transus (°C)	Temperature range (°C)	Q (kJ/mol)
IMI 834 [10]	1040	900–950	416
		950–1020	803
		1020–1060	472
IMI 834 [14]	1045	950–1030	703
		1050–1125	153
Ti 600 [35]	1010	800–1000	620
IMI 834 – current study	1060	850–1060	672

Table 4 Values of material constants estimated at various strain values for IMI 834 with a duplex starting microstructure.

Strain	Material constants			
	n	Q (kJ/mol)	α'	ln A
0.1	2.12	723	0.0175	64.31
0.2	2.14	690	0.0181	60.65
0.3	2.21	664	0.0185	58.74
0.4	2.24	663	0.0189	58.58
0.5	2.25	672	0.0198	59.51

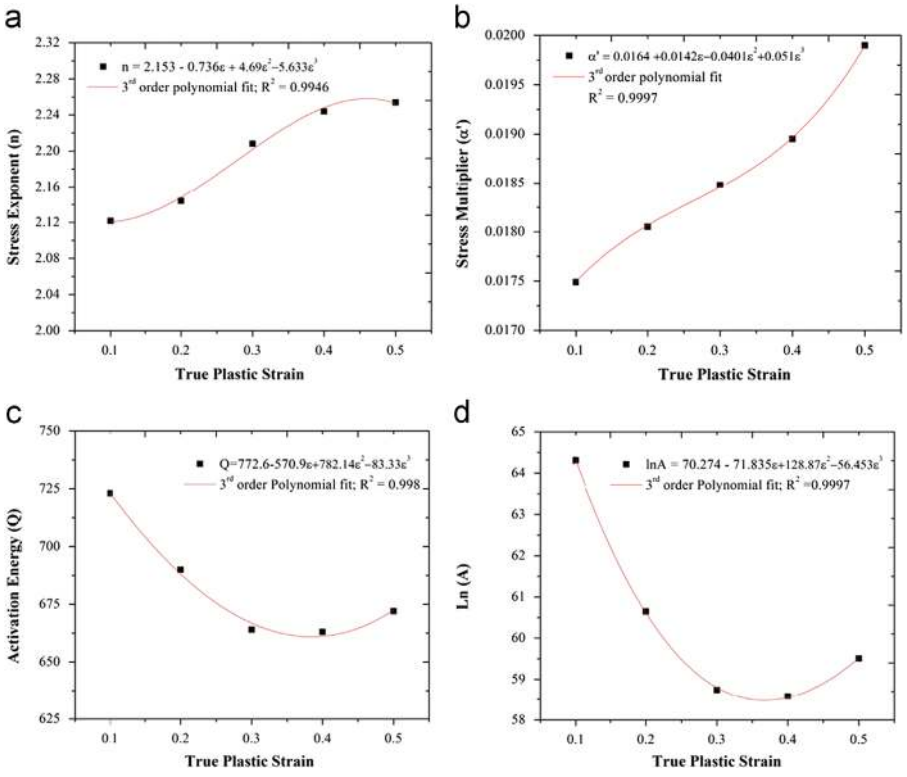

Fig. 9 Variation of (a) stress exponent, (b) stress multiplier, (c) activation energy and (d) ln(A) with strain.

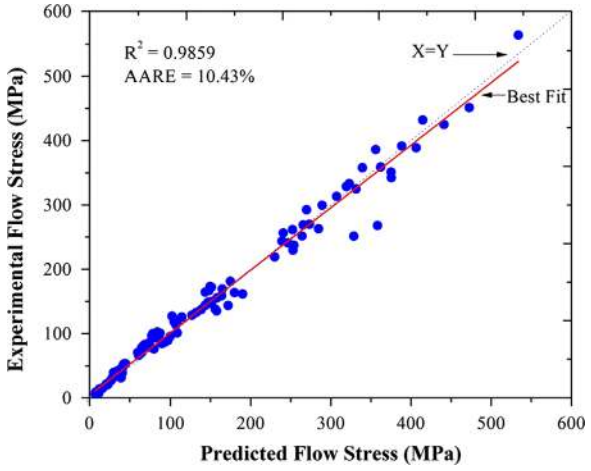

Fig. 10 Correlation between the experimental and predicted flow stress.

term by term comparison of the experimental and predicted flow stress and therefore is an unbiased statistical parameter for determining the predictability of Eq. (17). As shown in Fig. 10, the values of R^2 and AARE were found to be 0.9859 and 10.43% respectively. This implies that the established strain compensated statistical equation can be used to predict the flow stress and simulate the high temperature deformation behavior of the material on a reliable basis.

6. Conclusions

Based on the modeling studies carried out it can be concluded that

- The instability region lies between 850 and 900°C and $10^{-1} - 1/s$ where the material exhibits shear bands.
- The material exhibits two potential domains for processing; pseudo-superplastic domain between 925 and 975°C and $10^{-3} - 10^{-2}/s$ where the material undergoes continuous dynamic recrystallization (CDRX) or globularisation of lamellar alpha and a discontinuous dynamic beta recrystallization (DDRX) domain between 980 and 1020°C and $10^{-2} - 10^{-1}/s$. Either of these domains can be used to produce various components depending on the equipment available and the final microstructure and property required.
- The strain compensated Sellars–Tegrat constitutive equation established can be used to estimate the flow stress of the material on a reliable basis.

Acknowledgments

The authors express their gratitude to Dr. Amol A. Gokhale, Director, Defence Metallurgical Research Laboratory (DMRL) for permitting us to publish this work. Authors acknowledge the support rendered by Dr. A.K. Gogia, Division Head, Aeronautical Materials Division, DMRL in carrying out this work. Authors acknowledge the funding provided by Defence Research and Development Organisation (DRDO) to carry out the work.

References

[1] D.F. Neal, VIII World Conference on Titanium, Birmingham, U.K., 1995, pp. 2195–2204.
[2] D.F. Neal, VI World Conference on Titanium, France, 1998, pp. 253–258.
[3] T.W. Farthing, VI World Conference on Titanium, France, 1998, pp. 37–48.
[4] T. Noda, M. Okabe, S. Isobe, S. Nishikiori, H. Hattori, VIII World Conference on Titanium, Birmingham, U.K., 1995, pp. 2258–2264.
[5] Y. Honnorat, VI World Conference on Titanium, France, 1998, pp. 365–379.
[6] I. Balasundar, M. Sudhakara Rao, M.K. Rohatgi, T. Raghu, B.P. Kashyap, J. Mach. Form. Technol. 2 (2010) 141–156.
[7] R.R. Boyer, Mater. Sci. Eng. A 213 (1996) 103–114.
[8] B.P. Bewlay, M.F.X. Gigliotti, F.Z. Utyashev, O.A. Kaibyshev, Mater. Des. 21 (2000) 287–295.
[9] B.P. Bewlay, M.F.X. Gigliotti, F.Z. Utyashev, O.A. Kaibyshev, J. Mater. Process. Technol. 135 (2003) 324–329.
[10] P.S. Bate, P.L. Blackwell, J.W. Brooks, VI World Conference on Titanium, France, 1998, pp. 287–292.
[11] P. Wanjara, M. Jahazi, H. Monajati, S. Yue, J.P. Immarigeon, Mater. Sci. Eng. A 396 (2005) 50–60.
[12] P. Wanjara, M. Jahazi, H. Monajati, S. Yue, Mater. Sci. Eng. A 416 (2006) 300–311.
[13] P. Vo, M. Jahazi, S. Yue, P. Bocher, Mater. Sci. Eng. A 447 (2007) 99–110.
[14] P. Vo, M. Jahazi, S. Yue, Adv. Mater. Res. 89–91 (2010) 592–597.
[15] X. Wang, M. Jahazi, S. Yue, Mater. Sci. Eng. A 434 (2006) 188–193.
[16] M. Zhou, Mater. Sci. Eng. A 245 (1998) 29–38.
[17] H.M. Flower, Mater. Sci. Technol. 6 (1990) 1082–1092.
[18] C.Y. Gao, L.C. Zang, H.X. Yan, Mater. Sci. Eng. A 528 (2011) 4445–4452.
[19] S. Nemat-Nasser, W.G. Guo, V.F. Nesterenko, S.S. Infrakanti, Y.B. Gu, Mech. Mater. 33 (2001) 425–429.
[20] F.J. Zerilli, R.W. Armstrong, Proc. ASME (1995) 417–428.
[21] C.M. Sellars, W.J.McG. Tegart, Acta Metall. 14 (1966) 1136–1138.
[22] C.M. Sellars, W.J.McG. Tegart, Int. Metall. Rev. 17 (1972) 1–24.
[23] H.J. Mcqueen, N.D. Ryan, Mater. Sci. Eng. A 322 (2002) 43–53.
[24] S.L. Semiatin, V. Seetharaman, I. Wiess, Mater. Sci. Eng. A 263 (1999) 257–261.
[25] Hui-qin Chen, Chun-Xia Cao, Ling Guo, Lin Hai, Trans. Nonferrous Met. Soc. China 18 (2008) 1021–1027.
[26] R.M. Poths, G. Angella, B.P. Wynne, W.M. Rainforth, S.L. Semiatin, H.J. Beynon, Metall. Trans. A 35 (2004) 2993–3001.
[27] Y.C. Lin, X.-M. Chen, Mater. Des. 32 (2011) 1733–1739.
[28] Dipti Samataray, Sumantra Mandal, A.K. Bhaduri, Comput. Mater. Sci. 17 (2009) 568–576.
[29] Y.V.R.K. Prasad, S. Sasidhara, Hot Working Guide – A Compendium of Processing Maps, ASM International, Ohio, 1997.
[30] A.K. Kalyan Kumar, Criteria for Predicting Metallurgical Instabilities in Processing (M.S thesis), Department of Metallurgy, Indian Institute of Science, Bangalore, 1987.
[31] H. Ziegler, Progress in Solid Mechanics, vol. 4, John Wiley & Sons, NY91–193.
[32] I. Balasundar, T. Raghu, B.P. Kashyap, Int. J. Mater. Form. http://dx.doi.org/10.1007/s12289-013-1150-y.
[33] I. Wiess, S.L. Semiatin, Mater. Sci. Eng. A 263 (1999) 243–256.
[34] H.L. Gegel, J.C. Malas, S.M. Doraivelu, V.A. Shende, ASM Metals Hand book, vol. 14, ASM International, Ohio, 417–438.
[35] Miaoquan Li, Hongsi Pan, Yingying Lin, Jia Luo, J. Mater. Process. Technol. 183 (2007) 71–76.
[36] Young Niu, Hongliang Hou, Miaoquan Li, Zhiqiang Li, Mater. Sci. Eng. A 492 (2008) 24–28.
[37] I. Weiss, F.H. Froes, D. Eylon, G.E. Welsch, Metall. Trans. A 17 (1986) 1935–1947.
[38] F.J. Humphreys, M. Hatherly, Recrystallization and Related Annealing Phenomena, 2nd ed. Elsevier, Oxford, 2004.
[39] N. Ridley, Z.C. Wang, G.W. Lorimer, VIII World Conference on Titanium, Birmingham, UK, 1995, pp. 604–611.